Graphitic Carbon Nitride with Extraordinary Photocatalytic Activity Under Visible Light Irradiation

Gebrehiwot Gebreslassie[1](✉), Pankaj Bharali[2], Gebremedhin Gebremariam[3], Assefa Sergawie[1], and Esayas Alemayehu[4]

[1] Department of Industrial Chemistry, College of Applied Sciences, Addis Ababa Science and Technology University, 16417 Addis Ababa, Ethiopia
gebrehiwot.gebreslassie@aastu.edu.et

[2] Department of Chemical Sciences, Tezpur University, Napaam, Tezpur 784028, India

[3] Department Chemistry, College of Natural and Computational Sciences, Mekelle University, 231 Mekelle, Ethiopia

[4] Faculty of Civil and Environmental Engineering, Jimma University, 378 Jimma, Ethiopia

Abstract. Catalytic activities of graphitic carbon nitride (g-C_3N_4) are restricted thanks to inadequate visible light absorption and high rate electron–hole recombination. In this work, we synthesized porous g-C_3N_4 using polycondensation process. Structural and physico-chemical characteristics of the prepared g-C_3N_4 materials were studied via XRD, DRS, PL, FTIR, Raman spectroscopy, SEM, BET and CHN elemental analyzer. The prepared samples exhibited surprising catalytic activity for the photo-oxidation of rhodamine-B (RhB) in visible light irradiation. From the fabricated g-C_3N_4 materials, the g-C_3N_4-550 showed photodegradation efficiency of 100% towards the RhB pollutant in water within 30 min. No appreciable decrease of the photocatalytic efficiency of g-C_3N_4 was observed up to five consecutive cycles, confirming the synthesized g-C_3N_4 was highly stable. Thus, this work gave a simple process for large scale production of highly visible light responsive and stable g-C_3N_4 materials used for environmental remediation.

Keywords: Graphitic carbon nitride · Porous materials · Photodegradation

1 Introduction

Recently, photocatalysts have been broadly intended for the elimination of carbon-based pollutants from aqueous media in addition to from the atmosphere owing to their properties of transforming light energy to chemical energy for facilitating decompose various toxic contaminants [1, 2]. All-embracing efforts have been made by numerous researchers on the way to prepare semiconductor materials for the photocatalytic response with an suitable band gap, counting metal-containing oxide, oxynitride and sulfide [3, 4]. Nevertheless, the search to unconventional photocatalyst with a relatively simple fabrication process and extraordinary activity is still underway [5].. Graphitic

M. A. Delele et al. (Eds.): ICAST 2020, LNICST 385, pp. 423–441, 2021.
https://doi.org/10.1007/978-3-030-80618-7_29

carbon nitride (g-C_3N_4) is one of the new class photocatalyst under exploration [6]. Triazine units (C_3N_3) and heptazine (C_6N_7) form the basic building blocks of g-C_3N_4 and are linked by planar amino groups to form prolonged networks. Tri-s-triazine rings are more stable building blocks of g-C_3N_4 than triazine [7]. The g-C_3N_4 has a 2D structure like to that of graphene and has chemical compositions of C, N, and with H atoms as impurity [8, 9]. Fascinating properties of g-C_3N_4 include proper band gap to absorb visible light, exceptional two-dimensional structure, nontoxic nature, biocompatibility, superb thermal stability, tunable electronic structure and simple process for mass production. As a result, g-C_3N_4 is currently in focus to its applications as a metal-free catalyst for photodegradation of different organic CO_2 reduction and fuel cells [10, 11]. The use of g-C_3N_4 has been restricted by its many drawbacks such as: (a) low surface area, (b) high rate of electron−hole recombination, and (c) medium band gap (2.7 eV, absorbs visible light less than 465 nm) [12].

Unlike photocatalysts containing metal that need expensive precursors for synthesis, the g-C_3N_4 can be prepared via thermal condensation of nitrogen-rich organic chemicals i.e. thiourea, melamine, cyanamide, urea, and dicyandiamide [8, 13]. Of these, cyanamide is costly and volatile, and its derivatives (melamine or dicyanamide) has low solubility. Thus, preparation of g-C_3N_4 using cyanamide and melamine precursors, is either costly or tough to operate [14]. For this reason, inexpensive and non-toxic urea is preferred source for g-C_3N_4 fabrication for targeted structural and photcatalytic properties [15]. For instance, Lee et al. [16] had prepared meso-porous C_3N_4 from urea by a thermal polymerization procedure using silica nano-spheres as template and used for phenol removal. Recently, Fang et al. [17] reported g-C_3N_4 synthesized by directly heating urea for 2 h at 600 °C.

Herein, we report simple preparation of porous g-C_3N_4 through direct pyrolysis of the urea precursor at temperature alternating from 470 °C to 550 °C. This energy-saving process takes just 1 h to complete (Fig. 1). Several authors had reported that the temperature requirement of the g-C_3N_4 synthesis from urea were from 400 °C to 650 °C while the reaction time varied from 2 h to 4 h [14, 18, 19]. Undoubtedly, the

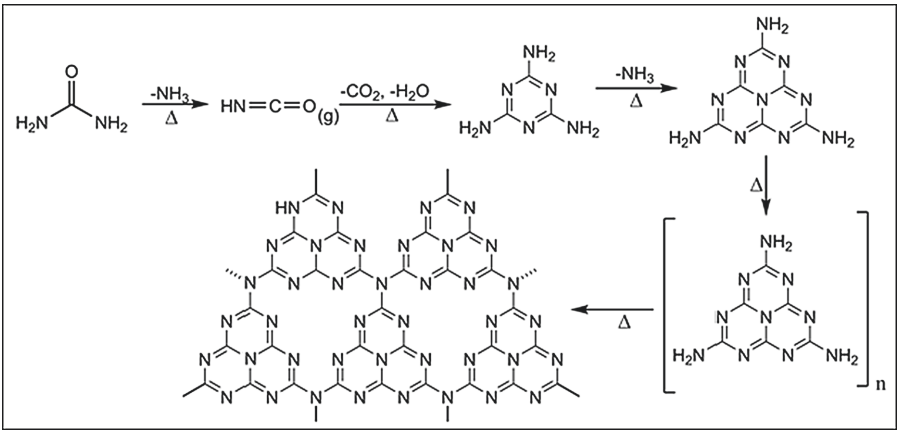

Fig. 1. Reaction diagram of the prepared g-C_3N_4 materials.

energy consumption was higher in those efforts. Following Fig. 1, the g-C_3N_4 obtained from heating of urea at 550 °C revealed extraordinary photodegradation towards RhB pollutant in aqueous solution. Notably, complete degradation of RhB ($C_o = 10$ mg L^{-1}) was achieved within 30 min in visible light treatment, using only 55 mg dose of catalyst. This can be attributed to the narrower band gap (2.5 eV), lower photogenerated electron-hole recombination rate and enhanced adsorption capability of the photocatalyst (due to large specific surface area 114.5 m^2 g^{-1}). Such a simple preparation method combined with superior photodegradation performance and confirmed long-term photostability may accelerate the use of g-C_3N_4 in practical environmental remediation protocols.

2 Experimental Part

2.1 Materials

Urea (CH_4N_2O, 99.5%), and nitric acid (HNO_3, 68%) were bought from Merck, India. Rhodamine B (RhB, 99.9%) was got from Rankem Fine Chemicals Pvt. Ltd., India. All the materials were used as obtained.

2.2 Preparation of g-C_3N_4

Graphitic carbon was prepared by poly-condensation of low-priced urea. In brief, optimized weight of urea (6 g) was kept in a ceramic crucible with cover and placed in a furnace and heated up to three different temperatures (470, 510 and 550 °C) for 1h. Thereafter, the crucible was permitted to cool to ambient temperature naturally. Then, products were ground into powder and washed with 0.1 M HNO_3 and distilled water. Finally, the products were dried at 60 °C and labeled as g-C_3N_4-470, g-C_3N_4-510 and g-C_3N_4-550 (tagged with the temperatures of preparation, for easy identification). The average weight of the g-C_3N_4 powders obtained from 6 g urea at 470, 510 and 550 °C were 0.535, 0.420 and 0.367 g, respectively.

2.3 Characterization Techniques

The crystallinity and orientation of the samples were studied using a D8 Focus Powder diffractometer (Bruker AXS, Germany). DRS results were noted using a UV–V is spectrometer (UV-2450, Shimadzu, Japan) within 200 nm to 900 nm. PL spectra were recorded using a Fluorescence spectrometer (LS 55, PerkinElmer) in 365 nm. IR spectra were recorded in FT-IR mode using a Frontier MIRFIR spectrometer (PerkinElmer), scanned over 400 to 4000 cm^{-1} in transmission mode. The Raman results were measured using Raman spectrometer (EZRRAMAN-N, EnwareOptronics, USA). Measurement was conducted in excitation laser 785 nm, NA0.3, spot size 3 μm, exposure time 10 s, pixel resolution 1.45 cm−1 per pixel, spectral region 3000–100 cm^{-1}. The elemental analysis was performed using a CHN Analyzer (2400 Series 2, PerkinElmer, USA). Nitrogen adsorption-desorption isotherm measurements were performed on a surface area analyzer (NOVA 1000E, Quantachrome). Before analysis, the sample was pretreated by degassing for 4 h at 150 °C to remove any adsorbed species. The specific

surface area of the photocatalyst was calculated from N_2 adsorption-desorption isotherm measurements using BET equation. Poresize distribution was got from the desorption branches through Barrett–Joyner–Halenda (BJH) method. Scanning electron microscopy was performed using a SEM (JSM 6390LV, JEOL, JAPAN). Elemental mapping was performed using JOEL JSM 6390LV equipped with EDS.

2.4 Photocatalytic Test

The photocatalytic ability of the g-C_3N_4 was assessed by RhB degradation in visible light irradiation. Normally, 55 mg of g-C_3N_4 photocatalyst was suspended in RhB solution (100 mL, 10 mg L^{-1}). The solution was stirred for 30 min in dark to confirm the formation of an adsorption-desorption equilibrium. Then, the mixture solution was illuminated with 10 W LED lamp (Havells, India). 3 mL aliquots were withdrawn at given time intervals of irradiation. The absorbance of the solution was measured using the UV−Vis spectrophotometer (Carry 60 UV-Vis, Agilent) at 554 nm corresponding to the maximum absorption wavelength of RhB after separated the photocatalyst using a centrifuge. The effects of amount catalyst, dye concentration, type of catalyst and catalyst stability were studied. The degradation efficiency was calculated using Eq. 1. Here, De is the degradation efficiency; C_o is the initial concentration of the RhB before irradiation and C represents the concentration of RhB after irradiation at time t. C and C_o values of RhB solution was calculated using Beer–Lambert ($A = \varepsilon bC$). First, we have been prepared calibration curve using RhB standard solutions and ε was obtained from the slope of A vs. C calibration curve. Then, the initial concentration (C_o) and concentration at a time t (C) of RhB were calculated using $C_o = A_o/\varepsilon b$ and $C = A/\varepsilon b$, respectively.

$$D_e = \frac{C_o - C}{C_o} \times 100 \tag{1}$$

2.5 Detection of the Reactive Species

Main active species were detected by active species trapping experiments. The detection process was same with the photocatalysis experiment. formic acid (FA, h^+ scavenger)p-benzoquinone (BQ, $\bullet O_2^-$ radical scavenger), and 2-propanol (2-PA, •OH radical scavenger) were added into photocatalytic system before the photocatalytic reaction happened in visible light illumination and the concentration of the scavengers was controlled to be fixed at 5 mol L^{-1}.

2.6 Recyclability and Stability Study

Recyclability and stability study were conducted by recovering and reused the g-C_3N_4 after photocatalysis reaction completed. Typically, after first photodegradation reaction completed, the g-C_3N_4 photocatalyst was recovered by centrifugation (5,000 rpm, 10 min) in an 800B centrifuge. Then, recovered g-C_3N_4 was washed 3 times by distilled water to remove adsorbed RhB and dried for 30 min. Thereafter, the dried g-C_3N_4 was reused for next photocatalytic reaction cycle. The stability study was conducted at optimum conditions; irradiation time (30 min), dosage of photocatalyst (55 mg) and concentration of RhB (10 mg L^{-1}).

3 Results and Discussion

3.1 Material Characterization

Crystal Structure, Surface Texture and Microstructure Analysis. In order to identify the factors affecting the main reaction of converting urea into g-C_3N_4, we examined the effect of covered or opened crucible and temperature effect. In covered crucible yellow colored solid was produced at a temperature above 400 °C as shown in Fig. 2a. Alternatively, when the crucible was open, no solid was produced and all the urea got decomposed into gaseous products. This is because in the opened crucible all the gases quickly escaped from the system without further reaction and condensation. Formation of $NH_{3(g)}$ at low temperatures during the pyrolysis reaction inside the covered crucible is essential as self-supporting atmosphere to initiate the polymerization of the intermediates into g-C_3N_4. The release of the $H_2O_{(g)}$ and $CO_{2(g)}$ during further condensation at high temperature contributed to exorcize the oxygen from the g-C_3N_4 product [20, 21]. In the covered crucible, the g-C_3N_4 solid could be produced up to annealing temperature of 550 °C (Fig. 2b). No solid was observed at temperatures greater than 550 °C, which showed that the g-C_3N_4 was completely decomposed during pyrolysis, even in a covered crucible, if the reaction temperature exceeded 550 °C.

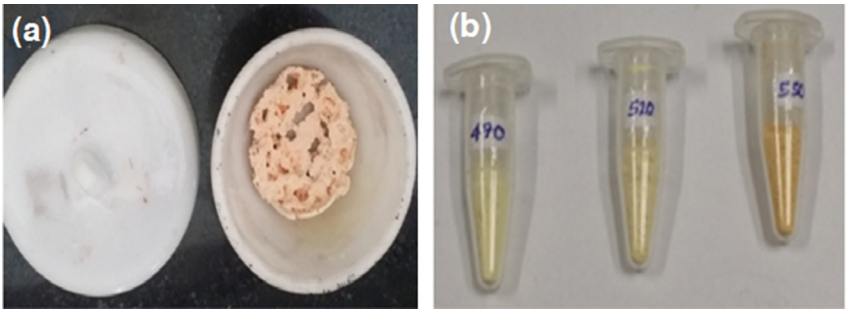

Fig. 2. (a) Photo of g-C_3N_4 prepared in a covered crucible with 6 g urea at 550 °C. (b) Photo of g-C_3N_4 samples prepared at 470, 510 and 550 °C, respectively.

Afterward, we studied the temperature effect on the structure of g-C_3N_4. Figure 3 demonstrations the XRD results of g-C_3N_4-470, g-C_3N_4-510 and g-C_3N_4-550 samples. The small angle peaks at $2\theta = 12.65°$ attributed to (100) planes of g-C_3N_4 and conforming to in-planar ordering of the nitrogen-linked tri-s-triazine units. For the two samples, g-C_3N_4-470 and g-C_3N_4-510, the 12.65° peak did not show any shift. On the other hand, the XRD peak at 12.65° shifted to 12.74° for the g-C_3N_4-550 sample (prepared at 550 °C). The strongest peak at $2\theta = 27.26°$ of the g-C_3N_4-470 sample shifted to 27.37° (in g-C_3N_4-510) and to 27.52° (in g-C_3N_4-550). These observations bring out the influence of preparation temperature on the XRD patterns. The interlayer stacking of the (002) planes in the g-C_3N_4 is strongly affected when the preparation temperature varied from 470 to 510 to 550 °C, causing the position shift of the strongest XRD peak. The slight shift of the (100) and (002) diffraction peaks toward higher diffraction angles

is associated to increased sample preparation temperature. It was reported by Praus et al. [22] that the increasing condensation temperature improved the polycondensation of g-C_3N_4. The crystallite size (D_{hkl}) were calculated by Scherrer's equation (Eq. 2).

$$D_{hkl} = \frac{\kappa\lambda}{\beta \cos\theta} \tag{2}$$

$$d_{hkl} = \frac{\lambda}{2 \sin\theta} \tag{3}$$

Where, λ is the wavelength of the X-rays (λ = 0.154 nm), β is the broadening diffraction peak at its FWHM, θ is the angle of diffraction and κ is a constant (i.e. 0.94). The average g-C_3N_4 crystallite sizes were estimated from the highest diffraction peaks (002) plane as $D_{002} = 5.92$ nm, $D_{002} = 6.20$ nm and $D_{002} = 7.13$ nm, corresponding to g-C_3N_4-470, g-C_3N_4-510 and g-C_3N_4-550 samples, respectively. The interlayer distance (d_{khl}) was calculated by using Eq. 3. The calculated interlayer spacing of the (002) planes was $d_{002} = 0.32$ nm and that of the (100) planes was $d_{100} = 0.69$ nm; these values are identical to g-C_3N_4-470, g-C_3N_4-510 and g-C_3N_4-550 samples. These results are in accordance with those previously reported results [22].

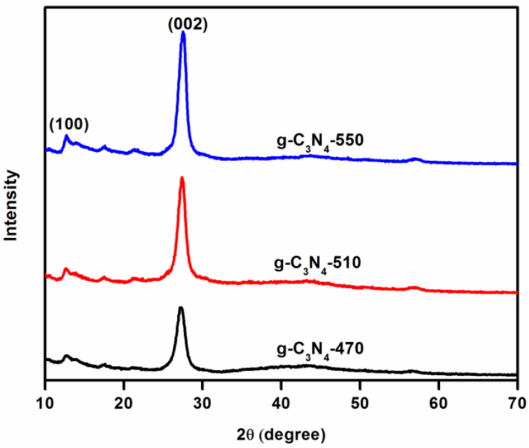

Fig. 3. XRD patterns for g-C_3N_4-470, g-C_3N_4-510 and g-C_3N_4-550 materials.

FT-IR analysis was accustomed characterize the molecular group in the prepared g-C_3N_4 samples. As presented in Fig. 4, the broad absorption bands at 3086, 3155 and 3252 cm^{-1} point out the presence of N−H and –NH_2 bonds. The distinctive skeletal vibrations of nitrogen hetero-cycles which match to stretching vibrations of C = N and C−N appear in between 1640 to 1235 cm^{-1}. The intensive bands at 1461, 1572, 1537 and 1640 cm^{-1} are ascribed to stretching of C = N. In addition, the stretching vibrations of C−N are characterized by the bands at 1235, 1316 and 1407 cm^{-1} [23]. In addition, the band at 812 cm^{-1} is recognized to heptazine units breathing mode, which found the energetically favored structure entities of g-C_3N_4 [24].

Furthermore, the surface textural properties of the g-C_3N_4 photocatalyst were characterized using nitrogen adsorption–desorption experiments. Specific surface area of g-C_3N_4-550 was calculated using BET method while the porosity property of the samples was calculated using the BJH method. As presented in Fig. 5a, the g-C_3N_4-550 possesses characteristic of mesoporous materials. The surface area of the g-C_3N_4-550 sample was found to be 114.5 m^2 g^{-1}. The BJH pore-size distribution graph (Fig. 5b) expresses that the g-C_3N_4–550 has pore-size distribution between 1 and 130 nm with pore diameter and pore volume of 3.98 nm and 1.43 m^3 g^{-1}, respectively.

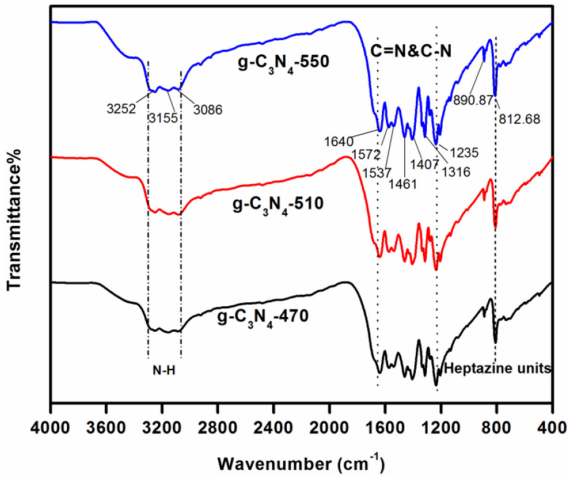

Fig. 4. The FTIR Spectra of the g-C_3N_4-470, g-C_3N_4-510 and g-C_3N_4-550 samples.

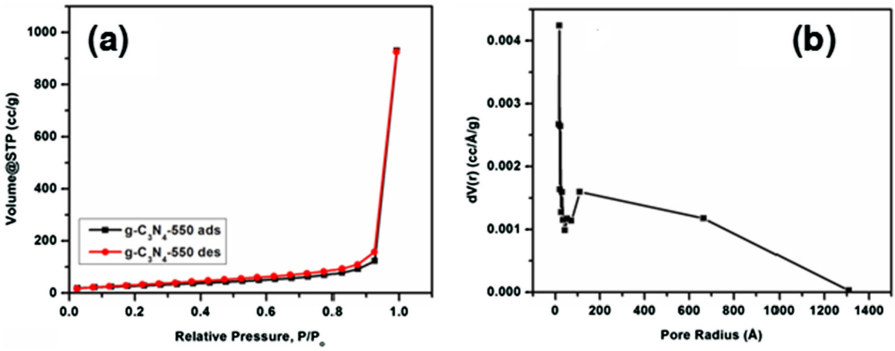

Fig. 5. (a) N_2 adsorption–desorption isotherm of the g-C_3N_4-550 sample. (b) The BJH pore-size distribution of the g-C_3N_4-550 sample.

Surface morphology and textural properties of the photocatalyst was investigated using a SEM. SEM images of g-C_3N_4-550 sample with different morphologies are represented in Fig. 6a–c. The agglomerated sheet like g-C_3N_4-550 was clearly observed.

EDS examination of g-C_3N_4 showed that the g-C_3N_4 consists of only C and N, which indicating that there is no impurity in the prepared g-C_3N_4 samples (Fig. 6d).

The Raman spectra results of g-C_3N_4 products were displayed in Fig. 7. As shown in Fig. 7, the Raman peaks at 712 and 1380 cm^{-1} are the features of typical g-C_3N_4. The spectral region of 1250–400 cm^{-1} is representative of skeletal vibrations of nitrogen based aromatic rings [25]. On the other hand, the common peak at 970 cm^{-1} confirmed skeletal vibration of heptazine. The strongest peak at 1380 cm^{-1}, observed in all the three samples, approves with the conversion urea to g-C_3N_4. The distinctive peak of g-C_3N_4 at about 712 cm^{-1} was also observed in all samples [26].

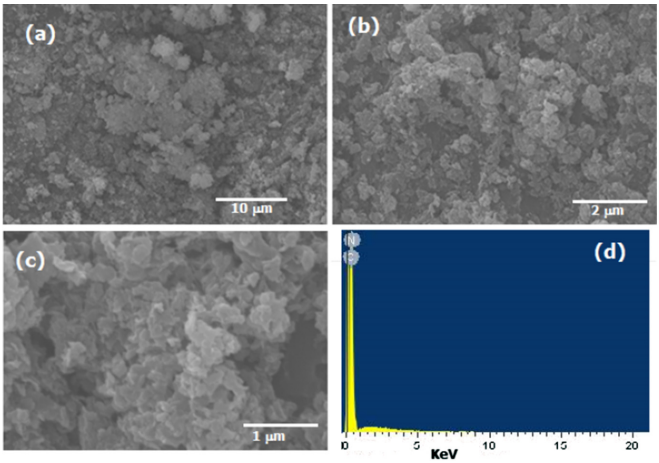

Fig. 6. (a-c) SEM images of the g-C_3N_4-550 sample at different magnifications. (d) The EDS spectrum for elemental compositions of the g-C_3N_4-550 sample.

Elemental Analysis. To further analyze the purity of the g-C_3N_4 photocatalysts, we carried out a composition check using the CHN analyzer technique. The results are summarized in Table 1. The data attest all of the three g-C_3N_4 samples contained C and N with a momentous amount of hydrogen. As preparation temperature was increased from 470 to 550 °C, the hydrogen content in the sample got decreased. The further decrease of hydrogen was due to the removal of hydrogen in the form of $NH_{3(g)}$ and $H_2O_{(g)}$. Nonetheless, the relatively high content of H_2 indicates the formation of $C_aN_bH_c$ sheets alongside with terminal -NH and -NH_2 groups, instead of the theoretical C_3N_4 (or C_6N_8) sheets, which are in accord with the FTIR results. The C:N molar ratio in the three samples depends strongly on the annealing temperature (Fig. 8). The C:N values of g-C_3N_4-470, g-C_3N_4-510 and g-C_3N_4-550 are 0.65, 0.67 and 0.72, respectively. This indicates that as the annealing temperature increases the C:N ratio increases (due to the removal of hydrogen from the sample). The maximal C:N ratio was found to be 0.72, which is almost proximate to the theoretical value of 0.75 for g-C_3N_4 [27]. Due to incomplete condensation of the urea, even at a temperature of 550 °C, the formula of g-$C_{6.3}N_{8.7}H_{2.5}$ (or, g-$C_{2.5}N_{3.5}H$) is more realistic than the g-C_3N_4. Regardless of this, graphitic carbon nitride is denoted as g-C_3N_4 for the sake of clarity and simplicity.

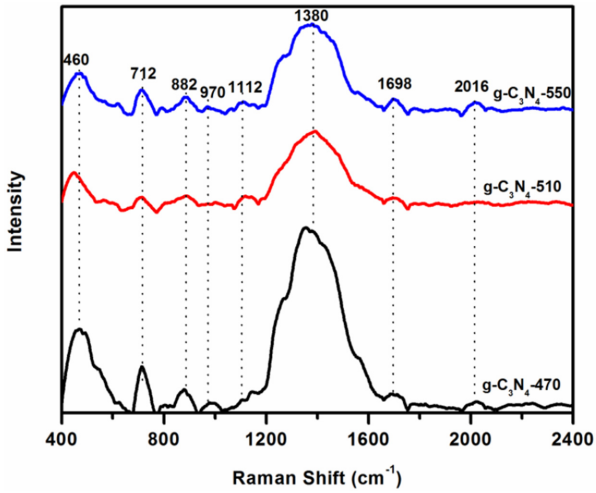

Fig. 7. The Raman spectra of the three g-C_3N_4 samples.

Table 1. CHN analysis and empirical composition of the g-$C_aN_bH_c$ samples.

Catalyst	C (wt%)	N (wt%)	H (wt%)	a	b	C
g-C_3N_4-470	33.97	64.02	2.01	5.66	9.14	3.98
g-C_3N_4-510	35.51	63.51	1.70	6.01	8.95	3.53
g-C_3N_4-550	37.65	61.07	1.28	6.27	8.72	2.53

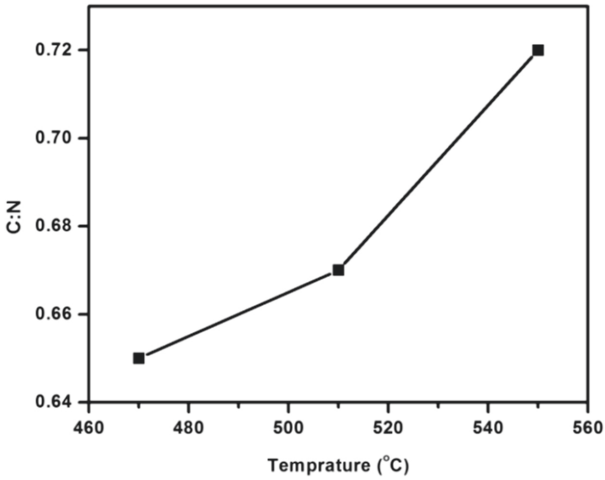

Fig. 8. C:N molar ratio of the g-C_3N_4 products at three different temperatures.

Optical and Photoluminescence Properties. The optical absorption properties of the prepared samples were investigated using DRS in 200–900 nm wavelength range. The plots in Fig. 9a indicate that the photo-absorption of g-C_3N_4 samples gets red-shifted after the preparation temperature increased from 470 °C to 550 °C. Absorption edge of g-C_3N_4-470, g-C_3N_4-510 and g-C_3N_4-550 were at about 473, 502 and 498 nm, respectively. This inferred that the prepared g-C_3N_4 samples can absorb solar energy up to 503 nm. The E_g of g-C_3N_4 was calculated using Eq. 4.

$$\alpha h\nu = k(h\nu - E_g)^{\frac{n}{2}} \tag{4}$$

Where, α is absorption coefficient, h is Planck's constant, ν is frequency of the absorbing light, E_g is band gap energy; k is a proportionality constant and n is constant number (i.e. 1 for direct and 4 for indirect band gap transition material). As can be seen in Fig. 9b, the indirect band gap (E_g) values of the g-C_3N_4-470, g-C_3N_4-510 and g-C_3N_4-550 are 2.62, 2.47 and 2.5 eV, respectively. As a result, the g-C_3N_4 is expected to own remarkable photocatalytic activity under the visible-light irradiation.

The recombination rate of e^-/h^+ pairs was examined from PL emission intensity. Figure 10 displays the PL spectra of the g-C_3N_4-470, g-C_3N_4-510 and g-C_3N_4-550 photocatalysts. The spectrum intensity for the g-C_3N_4-550 is lower than the corresponding g-C_3N_4-470 and g-C_3N_4-510 samples. One may understand that the recombination rate of e^-/h^+ pairs in g-C_3N_4-550 is lower than that of the g-C_3N_4-470 and g-C_3N_4-510 materials. Hence, the photogenerated charge carriers in the g-C_3N_4-550 could have longer lifetime and they can freely participate in the photocatalytic reactions. Thus, based on the obtained results from DRS and the PL, the g-C_3N_4-550 sample is predictable to exhibit catalytic enhancement than the g-C_3N_4-470 and g-C_3N_4-510.

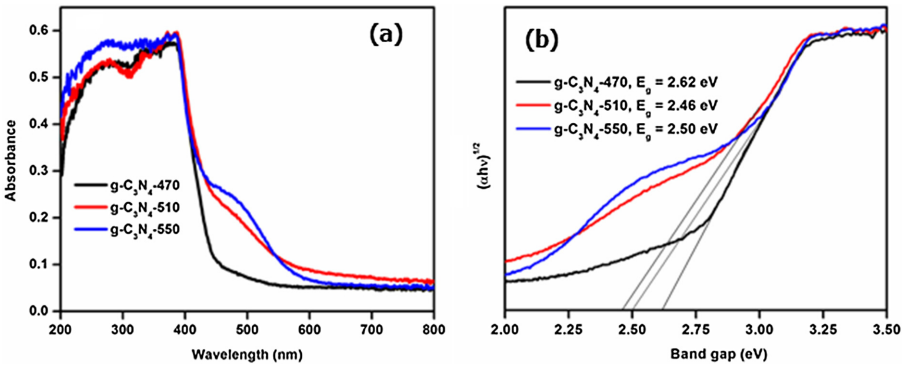

Fig. 9. (a) The UV–VIS DRS for the g-C_3N_4 samples. (b) Estimated indirect band gaps of the g-C_3N_4 samples.

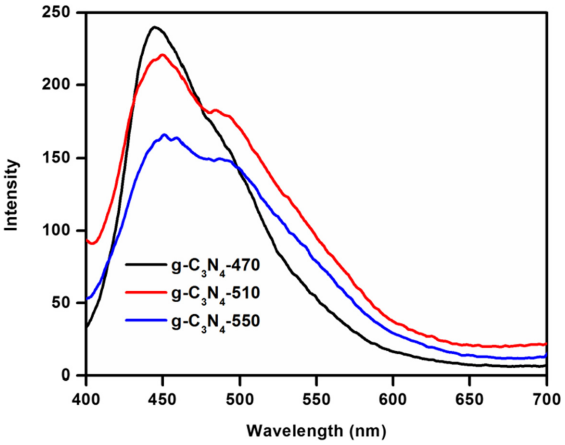

Fig. 10. The photoluminescence (PL) spectra of the g-C3N4-470, g-C3N4-510 and g-C3N4-550 samples at an excitation wavelength of 365 nm.

3.2 Photocatalytic Activity

Effect of Catalyst Dosage. Investigation were accomplished by changing the amounts of g-C_3N_4-550 photocatalyst, keeping the RhB concentration fixed (10 mg L^{-1}, 100 mL). During adsorption-desorption experiment in dark place, decreasing in dye concentration was observed as the catalyst loading increases from 15 to 65 mg in the first 15 min (Fig. 11a). This is due to the amount of the dye adsorbed on the catalyst increases as the catalyst dose increases (i.e. active sites increase). Then, the dye concentration is constant during 15 to 30 min and adsorption-desorption equilibrium reached 30 min. After visible light irradiation, the rate of reaction increased when the amount of g-C_3N_4 photocatalyst increased from 15 to 55 mg, beyond which it showed a reduction (Fig. 11a). As displayed in Fig. 11b, the efficiency of RhB degradation increased as the catalyst dose increased. The enhanced degradation may be attributed to an increase of the number of active sites of catalyst which accelerates the photoreaction. The lower rate (when the catalyst dosage is increased beyond 55 mg) is due to the scattering of the light in the reaction mixture, which delays light penetration through the solution containing the RhB. Similarly, with a higher dose of catalyst, the possibility of deactivation of the activated molecules by the ground state molecules (through collision) is very high and this causes a decreases in the rate of reaction [28]. Thus, the optimum dosage of the g-C_3N_4 photocatalyst for the RhB degradation reaction may be taken as 55 mg.

Effect of Initial RhB Concentration. The influence of initial concentration of RhB on degradation rate was investigated by varying RhB concentration from 5 mg L^{-1} to 15 mg L^{-1}, keeping amount of g-C_3N_4-550 (55 mg per 100 mL of the reaction mixture) constant. The degradation efficiency was almost the same even if the RhB concentration increased from 5 to 10 mg L^{-1}. However, it is decreased after RhB concentration increased beyond 10 mg L^{-1} (Table 2). Thus, the optimum RhB concentration in the reaction mixture was taken as 10 mg L^{-1}.

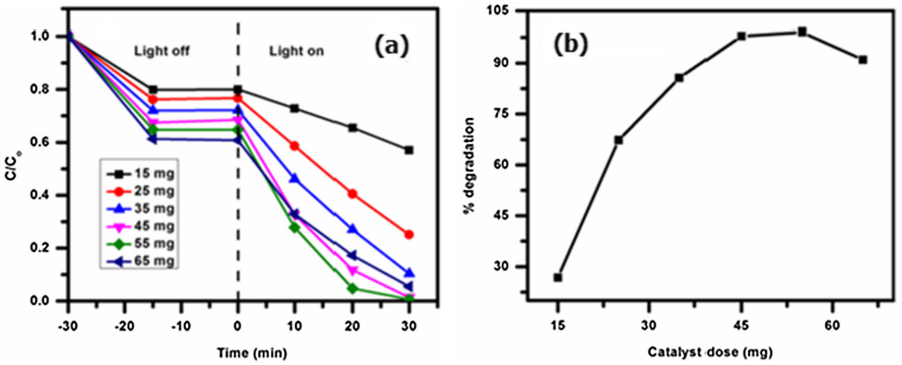

Fig. 11. (a) Effect of dose of g-C_3N_4 on the photodegradation of RhB (RhB concentration: 10 mg L^{-1}) (b) Degradation efficiency of the RhB against the amount of g-C_3N_4 photocatalyst within 30 min.

Table 2. Effect of RhB concentration on the degradation rate.

g-C_3N_4 dose (mg)	RhB concentration (mg L^{-1})	RhB volume (mL)	%degradation	Time (min)
55	5	100	100%	30
55	10	100	100%	30
55	15	100	64%	30

Effect of Catalyst Type. The photocatalytic performance of the g-C_3N_4 catalysts prepared at different condensation temperatures (g-C_3N_4-470, g-C_3N_4-510 and g-C_3N_4-550) were tried for the degradation of RhB solution under visible light irradiation. Adsorption-desorption experiments were conducted as displayed in Fig. 12. As shown in Fig. 12, the adsorption RhB into g-C_3N_4-550 increases up to 15 min. However, the amount of RhB adsorbed on g-C_3N_4-550 within 15 min was the same as that of adsorbed within 30 min. This indicates the adsorption-desorption equilibrium was obtained within 30 min in a dark place and almost 35% of the RhB was adsorbed on g-C_3N_4-550 before the visible light illumination (see inset in Fig. 12). RhB degradation of was not observed without the catalyst under illumination of visible light (Fig. 13a). Further, in the being of the g-C_3N_4 catalyst, no degradation was observed in dark. This confirmed that the degradation of RhB takes place only when g-C_3N_4 photocatalyst is present under light illumination. Figure 13 b-d shows a series of plots of absorbance versus wavelength for degradation of RhB over g-C_3N_4-470, g-C_3N_4-510 and g-C_3N_4-550 samples. As shown, as the irradiation time increased, absorption intensity decreased. But, shift of RhB absorption peak (centered at 554 nm) was not observed. The efficiency of RhB pollutant degradation over the g-C_3N_4-470, g-C_3N_4-510 and g-C_3N_4-550 were found to be 93.9%, 97.3%, and 100%, respectively. Furthermore, the photocatalytic performance of our g-C_3N_4-550 photocatalyst was compared with previously reported urea derived g-C_3N_4. The present procedure showed an excellent photocatalytic performance which

required just 30 min for the complete degradation of RhB pollutant (10 mg L^{-1}) under visible light irradiation (10 W LED lamp) using 55 mg of g-C_3N_4.

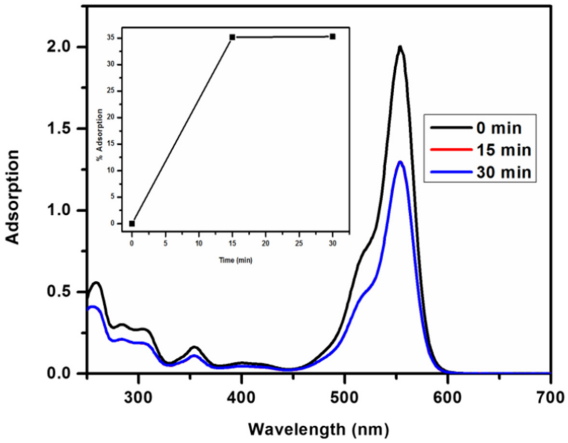

Fig. 12. Change of optical absorption of the RhB solution during adsorption in the dark. The inset shows the %Adsorption of RhB on the g-C_3N_4–550 in the dark.

According to the Langmuir–Hinshelwood model, the photodegradation of RhB over g-C_3N_4 photocatalysts fits pseudo-first-order kinetics (Eq. 5).

$$\ln\left(\frac{C_o}{C}\right) = k_{ap}t \tag{5}$$

Where, C_o is the initial RhB concentration before irradiation and C is the RhB concentration at time t after irradiation and k_{ap} is the apparent pseudo-first-order rate constant. It can be seen in Fig. 14, that there exists a linear relationship between $\ln(C_o/C)$ and t, confirming that the photodegradation reaction is definitely a pseudo-first-order reaction. The k_{ap} of the photodegradation reaction were estimated to be 0.0933, 0.1223 and 0.1539 min^{-1} for g-C_3N_4-470, g-C_3N_4-510 and g-C_3N_4-550, respectively. The highest value of k_{ap} further proven that the g-C_3N_4-550 had the highest photocatalytic activity amongst the three catalysts. The superior activity was related to more visible-light absorption, large surface area and better suppression of electron-hole pairs from their undesirable recombination.

Proposed Photocatalytic Degradation Mechanism. The mechanism of photocatalytic activity of g-C_3N_4 was proposed from Active species trapping experiments. As presented in Fig. 15, the addition of benzoquinone (BQ, $\bullet O_2^-$ scavenger) acutely reduce the RhB oxidation on g-C_3N_4, suggesting that $\bullet O_2^-$ are the main reactive species for the photooxidation of RhB. As an alternative, no obvious depression in photocatalytic efficiency was observed in the presence of 2-propanol (2-PA, •OH scavenger), suggesting that •OH does not participate as active species on the photocatalytic degradation process. The large improvement of the RhB photooxidation after addition of formic acid

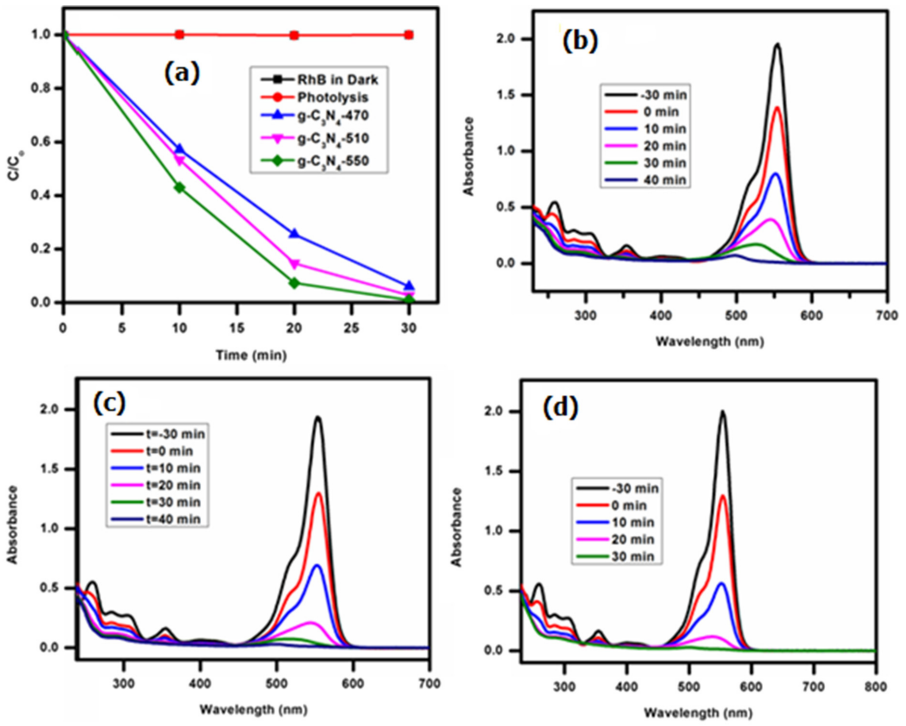

Fig. 13. (a) Photo-degradation of RhB over the g-C_3N_4-470, g-C_3N_4–510 and g-C_3N_4-550 photocatalysts. RhB degradation under irradiation of visible light (b) g-C_3N_4-470 (c) g-C_3N_4-510, and (d) g-C_3N_4-550. [RhB] = 10 mg L^{-1}, RhB volume 100 mL and catalyst dosage = 55 mg of reaction mixture.

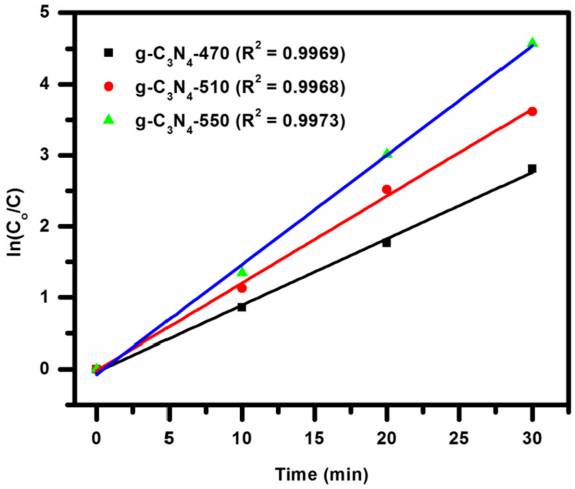

Fig. 14. Pseudo first-order kinetics of the RhB photodegradation reaction by the three photocatalysts.

(FA, h^+ scavenger) more confirmed that RhB is mainly oxidized by $\bullet O_2^-$, because the trapping of hole by FA would produce more photogenerated electrons by preventing the recombination of photogenerated e^-/h^+ pairs. The VB and CB positions for g-C_3N_4 are calculated and the values are +1.23 and −1.27 eV, respectively. The VB of g-C_3N_4 (+1.23 eV vs. NHE) is more negative compared with the E° of OH −/•OH (+1.99 eV vs. NHE) [29, 30]. That's why, the photogenerated h^+ in VB of g-C_3N_4 cannot oxidize the OH^- to produce •OH radicals. The CB of g-C_3N_4 (−1.27 eV vs. NHE) is more negative than the E° of $O_2/\bullet O_2^-$ (−0.33 eV vs. NHE) and hence can reduce the adsorbed oxygen molecules so as to yield $\bullet O_2$ that can oxidize the RhB [31]. This agrees the $\bullet O_2^-$ is the main reactive species take part in the photocatalytic RhB degradation of in the presence of g-C_3N_4. Therefore, based on the obtained results from the active species trapping experiment, and VB and CB edge positions of g-C_3N_4 photocatalyst, the photocatalytic reaction mechanism of RhB over g-C_3N_4 shown in Fig. 16 was proposed.

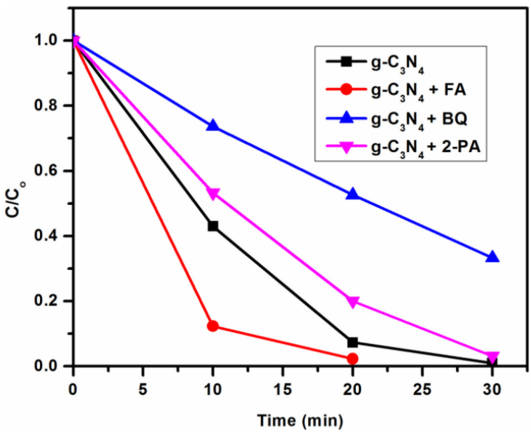

Fig. 15. Photocatalytic performance of g-C_3N_4 for the RhB degradation in the presence of different scavengers (BQ, 2-PA and FA).

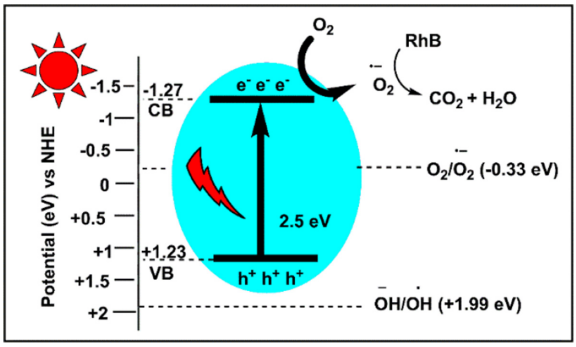

Fig. 16. Proposed mechanism of RhB degradation over the g-C_3N_4.

Stability of the Photocatalysts. The catalyst stability is very significant from the viewpoint of its practical application. So as to examine the stability of g-C_3N_4 photocatalyst, we accomplished the recycled RhB degradation in irradiation of visible light. As we can see in Fig. 17, the photocatalytic efficiency was almost the same for four successive cycles. But during the fifth consecutive cycle, it decreased by 5%, which may not be watched as a substantial decrease. Furthermore, the structural and optical properties of the g-C_3N_4 photocatalyst after catalytic reaction were examined using XRD, FTIR and DRS techniques. The XRD patterns, DRS and FTIR spectra of g-C_3N_4 before and after photodegradation of RhB are shown in Figs. 18 and 19. As shown in in Figs. 18 and 19, there were no appreciable changes in the structural and optical properties of the g-C_3N_4 samples before and after photodegradation experiments. It may then be decided that the g-C_3N_4 can be considered as a stable and highly active photocatalyst in visible light irradiation, suitable for use in photo-degrading organic pollutants.

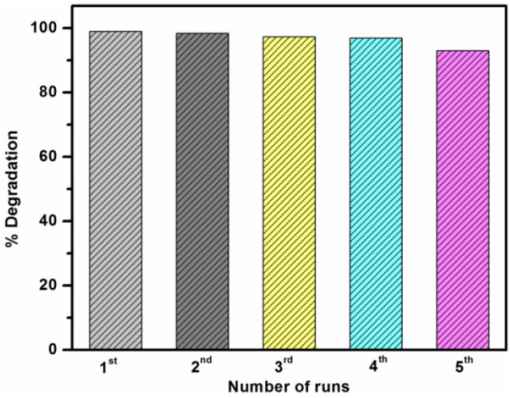

Fig. 17. Stability of g-C_3N_4 catalyst for five consecutive cycles.

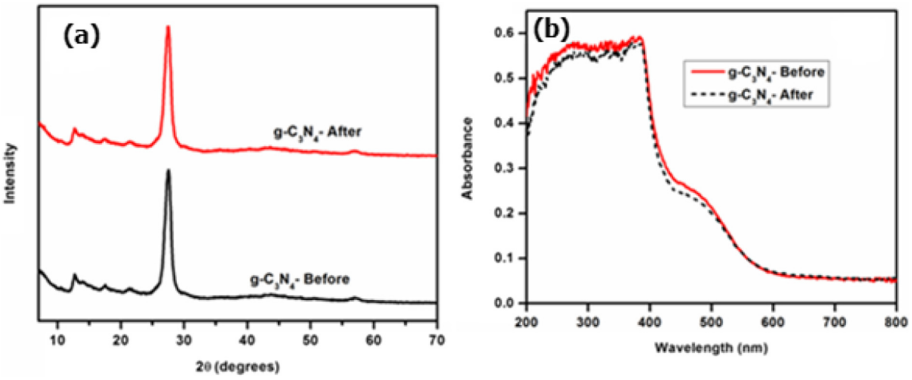

Fig. 18. (a) XRD patterns of g-C_3N_4 before and after photodegradation of RhB (after five cycles). (b) UV–VIS DRS spectra of g-C_3N_4 before and after photodegradation of RhB (after five cycles).

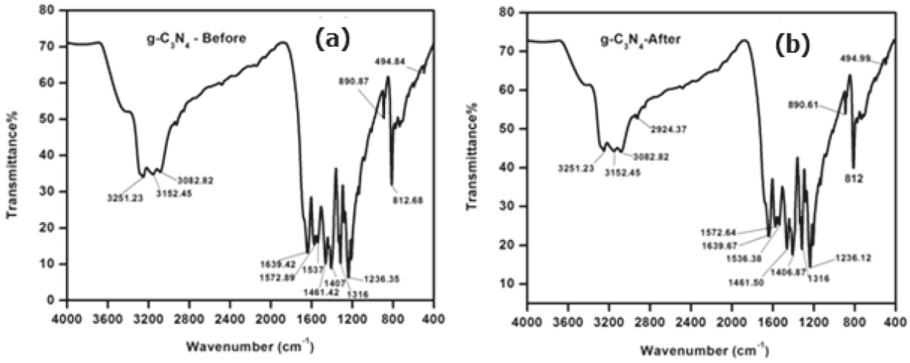

Fig. 19. The FTIR spectra for the g-C_3N_4 before and after photodegradation of RhB (after five cycles).

4 Conclusion

Graphitic carbon nitride (g-C_3N_4) materials with high surface area were excellently synthesized from urea via a polycondensation method at temperatures 470, 510 and 550 °C. Different characterization methods were used to investigate the physico-chemical and structural properties of the fabricated g-C_3N_4 materials. Photocatalytic activities of the samples were tested by the degradations of RhB in visible-light illumination. The g-C_3N_4–550 catalyst degraded the RhB pollutant within 30 min, with an efficiency of about 100%. Moreover, the prepared g-C_3N_4 photocatalysts had retained the same activity for five consecutive cycles. The outstanding photocatalytic performance of g-C_3N_4 was interrelated to a suitable band gap (2.5 eV) and high specific surface area (114.5 $m^2 g^{-1}$), in addition to low electron-hole recombination. Combined with a simple preparation method, a superior photodegradation activity and a durable photocatalytic stability of the g-C_3N_4 materials has generated significant interest in the photocatalytic degradation of organic poll utants.

References

1. Xu, Y., Xu, H., Wang, L., et al.: The CNT modified white C_3N_4 composite photocatalyst with enhanced visible-light response photoactivity. Dalt. Trans. **42**, 7604–7613 (2013)
2. Gebreslassie, G., Bharali, P., Chandra, U., et al.: Hydrothermal synthesis of g-C_3N_4/$NiFe_2O_4$ nanocomposite and its enhanced photocatalytic activity. Appl. Organomet. Chem. **33**, e5002 (2019). https://doi.org/10.1002/aoc.5002
3. Wajid Shah, M., Zhu, Y., Fan, X., et al.: Facile synthesis of defective TiO_{2-x} nanocrystals with high surface area and tailoring bandgap for visible-light photocatalysis. Sci. Rep. **5**, 15804 (2015)
4. Saputra, E., Muhammad, S., Sun, H., et al.: A comparative study of spinel structured Mn_3O_4, Co_3O_4 and Fe_3O_4 nanoparticles in catalytic oxidation of phenolic contaminants in aqueous solutions. J. Colloid. Interface Sci. **407**, 467–473 (2013)
5. Niu, P., Zhang, L., Liu, G., Cheng, H.M.: Graphene-like carbon nitride nanosheets for improved photocatalytic activities. Adv. Funct. Mater. **22**, 4763–4770 (2012)

6. Wang, A., Wang, C., Fu, L., Wong-Ng, W., Lan, Y.: Recent advances of graphitic carbon nitride-based structures and applications in catalyst, sensing, imaging, and LEDs. Nano-Micro Lett. **9**(4), 1–21 (2017). https://doi.org/10.1007/s40820-017-0148-2
7. Zheng, Y., Lin, L., Wang, B., Wang, X.: Graphitic carbon nitride polymers toward sustainable photoredox catalysis. Angew Chemie – Int. Ed. **54**, 12868–12884 (2015)
8. Sun, H., Zhou, G., Wang, Y., et al.: A new metal-free carbon hybrid for enhanced photocatalysis. ACS Appl. Mater. Interfaces **6**, 16745–16754 (2014)
9. Guo, F., Shi, W., Li, M., et al.: 2D/2D Z-scheme heterojunction of $CuInS_2$/g-C_3N_4 for enhanced visible-light-driven photocatalytic activity towards the degradation of tetracycline. Sep. Purif. Technol. **210**, 608–615 (2019)
10. Liu, J., Wang, H., Antonietti, M.: Graphitic carbon nitride "reloaded": emerging applications beyond (photo)catalysis. Chem. Soc. Rev. **45**, 2308–2326 (2016)
11. Xue, J., Ma, S., Zhou, Y., Wang, Q.: Au-loaded porous graphitic C_3N_4/graphene layered composite as a ternary plasmonic photocatalyst and its visible-light photocatalytic performance. RSC Adv. **5**, 88249–88257 (2015)
12. Zhao, Z., Sun, Y., Dong, F.: Graphitic carbon nitride based nanocomposites: a review. Nanoscale **7**, 15–37 (2015)
13. Gebreslassie, G., Bharali, P., Chandra, U., et al.: Novel g-C_3N_4/graphene/$NiFe_2O_4$ nanocomposites as magnetically separable visible light driven photocatalysts. J. Photochem. Photobiol. A Chem. **382** (2019)
14. Dong, F., Wu, L., Sun, Y., et al.: Efficient synthesis of polymeric g-C_3N_4 layered materials as novel efficient visible light driven photocatalysts. J. Mater. Chem. **21**, 15171–15174 (2011)
15. Cao, S., Low, J., Yu, J., Jaroniec, M.: Polymeric photocatalysts based on graphitic carbon nitride. Adv. Mater. **27**, 2150–2176 (2015)
16. Lee, S.C., Lintang, H.O., Yuliati, L.: A urea precursor to synthesize carbon nitride with mesoporosity for enhanced activity in the photocatalytic removal of phenol. Chem. - Asian J. **7**, 2139–2144 (2012)
17. Fang, H., Luo, Y., Zheng, Y., et al.: Facile large-scale synthesis of urea-derived porous graphitic carbon nitride with extraordinary visible-light spectrum photodegradation. Ind. Eng. Chem. Res. **55**, 4506–4514 (2016)
18. Shi, L., Liang, L., Wang, F., et al.: Higher yield urea-derived polymeric graphitic carbon nitride with mesoporous structure and superior visible-light-responsive activity. ACS Sustain. Chem. Eng. **3**, 3412–3419 (2015)
19. Zhang, Y., Liu, J., Wu, G., Chen, W.: Porous graphitic carbon nitride synthesized via direct polymerization of urea for efficient sunlight-driven photocatalytic hydrogen production. Nanoscale **4**, 5300–5303 (2012)
20. Ong, W.J., Tan, L.L., Ng, Y.H., et al.: Graphitic carbon nitride (g-C_3N_4)-based photocatalysts for artificial photosynthesis and environmental remediation: are we a step closer to achieving sustainability? Chem. Rev. **116**, 7159–7329 (2016)
21. Liu, J., Zhang, T., Wang, Z., et al.: Simple pyrolysis of urea into graphitic carbon nitride with recyclable adsorption and photocatalytic activity. J. Mater. Chem. **21**, 14398–14401 (2011)
22. Praus, P., Svoboda, L., Ritz, M., et al.: Graphitic carbon nitride: synthesis, characterization and photocatalytic decomposition of nitrous oxide. Mater. Chem. Phys. **193**, 438–446 (2017)
23. Pawar, R.C., Kang, S., Park, J.H., et al.: Room-temperature synthesis of nanoporous 1D microrods of graphitic carbon nitride (g-C_3N_4) with highly enhanced photocatalytic activity and stability. Sci. Rep. **6**, 1–14 (2016)
24. Shi, Y., Huang, J., Zeng, G., et al.: Stable, metal-free, visible-light-driven photocatalyst for efficient removal of pollutants: mechanism of action. J. Colloid. Interface Sci. **531**, 433–443 (2018)
25. Marchewka, M.K.: Infrared and Raman spectra of melaminium chloride hemihydrate. Mater. Sci. Eng. B **95**, 214–221 (2002)

26. Papailias, I., Giannakopoulou, T., Todorova, N., et al.: Effect of processing temperature on structure and photocatalytic properties of g-C_3N_4. Appl. Surf. Sci. **358**, 278–286 (2015)
27. Yan, S.C., Li, Z.S., Zou, Z.G.: Photodegradation performance of g-C_3N_4 fabricated by directly heating melamine. Langmuir **25**, 10397–10401 (2009)
28. Nagaraja, R., Kottam, N., Girija, C.R., Nagabhushana, B.M.: Photocatalytic degradation of Rhodamine B dye under UV/solar light using ZnO nanopowder synthesized by solution combustion route. Powder Technol. **215–216**, 91–97 (2012)
29. Li, Y., Zhang, H., Liu, P., et al.: Cross-linked g-C_3N_4/rGO nanocomposites with tunable band structure and enhanced visible light photocatalytic activity. Small **9**, 3336–3344 (2013)
30. Ye, L., Liu, J., Jiang, Z., et al.: Facets coupling of BiOBr-g-C_3N_4 composite photocatalyst for enhanced visible-light-driven photocatalytic activity. Appl. Catal. B, Environ. **142–143**, 1–7 (2013)
31. Mousavi, M., Habibi-Yangjeh, A., Seifzadeh, D., et al.: Exceptional photocatalytic activity for g-C_3N_4 activated by H_2O_2 and integrated with Bi_2S_3 and Fe_3O_4 nanoparticles for removal of organic and inorganic pollutants. Adv. Powder Technol. **30**, 524–537 (2018)